

# An Investigation of Wall-Proximity Effect Using a Typical Large-Scale Five-Hole Probe

**Sang Woo Lee\* and Tae Jin Yoon\*\***

(Received May 25, 1998)

Effects of wall proximity on the calibration of a typical cone-type five-hole probe with a cobra-shaped stem have been investigated for various probe-wall orientations with the variation of yaw angle. In order to obtain a negligibly small boundary-layer thickness to the probe-head diameter, a large-scale five-hole probe is employed in a well-established laminar boundary layer, and the probe Reynolds number is kept to be  $3.53 \times 10^4$ , which is a representative Reynolds number in turbomachinery flows. The wall-proximity effect, which is closely related to the complicated three-dimensional flow change due to the presence of the wall, is found to be pronounced only when the wall proximity is less than two times the probe-head diameter. In general, larger orientation angle between the wall and the probe head results in smaller wall-proximity effect in flow angle measurements. In this study, changes in the pitch and yaw angles due to the wall proximity are evaluated through a typical non-nulling reduction procedure. The results may provide a useful guideline in the near-wall measurement.

**Key Words:** Five-Hole Probe, Wall Proximity, Calibration, Non-Nulling Method, Large-Scale Cone Probe

wall or wall proximity, Fig. 3

## Nomenclature

$C_{pa}$  : Pitch-angle coefficient, Eq. (1)  
 $C_{sp}$  : Static-pressure coefficient, Eq. (3)  
 $C_{tp}$  : Total-pressure coefficient, Eq. (4)  
 $C_{ya}$  : Yaw-angle coefficient, Eq. (2)  
 $D$  : Diameter of the five-hole probe head  
 $P_{av}$  : Average pressure, Eq. (5)  
 $P_i$  : Pressure measured at the  $i$ -th pressure hole of the five-hole probe  
 $P_s$  : Static pressure  
 $P_t$  : Total pressure  
 $Re_D$  : Probe Reynolds number  $= U_\infty D / \nu$   
 $Re_x$  : Probe Reynolds number  $= U_\infty x / \nu$   
 $U_\infty$  : Freestream velocity  
 $x$  : Streamwise coordinate, Fig. 3  
 $y$  : Normal coordinate, Fig. 3  
 $y_p$  : Distance between the probe center and

## Greek character

$\alpha$  : Pitch angle, Fig. 1 or Fig. 3  
 $\alpha_\infty$  : Pitch angle without wall-proximity effect  
 $\beta$  : Yaw angle, Fig. 1 or Fig. 3  
 $\beta_\infty$  : Yaw angle without wall-proximity effect  
 $\delta_{99}$  : Boundary-layer thickness  
 $\nu$  : Kinematic viscosity  
 $\rho$  : Density

## 1. Introduction

A five-hole probe is a very useful means for the research and development of turbomachinery and is also extensively used in the measurement of complex three-dimensional flows encountered in various fluid engineering branches, because it directly provides static and total pressures as well as flow angles (Lee et al., 1994; Lee et al., 1997). In the research of the turbomachines, it is very important to understand the flow close to a solid wall, because strong secondary flows and aer-

\* Dept. of Mechanical Engrg., Kumoh National University of Technology

\*\* Graduate school, Kumoh National University of Technology

dynamic losses tends to be produced near the wall. The calibration of the five-hole probe is usually performed in a uniform flow out of a wind-tunnel exit. If the calibrated five-hole probe is located close to the wall in a uniform flow with a negligibly thin boundary layer in comparison with the probe diameter, the pressure measured at each pressure-sensing hole may be different from that measured at the location far away from the wall due to the probe-wall flow interaction. This is generally termed as "wall-proximity effect" (Treaster and Yocum, 1979). Thus, special care should be taken in applying the freestream calibration data to a near-wall measurement.

In general, a near-wall flow can have large yaw angle, but tends to be parallel to the wall, since the presence of the wall makes the flow aligned parallel with the solid surface. Therefore, the near-wall flow can not have velocity components departing from the wall and moving toward the wall. Actually, it is impossible to make these kinds of near-wall flow in a laboratory. In this study, it is assumed that the actual flow near the wall is always parallel to the wall at the locations where the wall-proximity effect is important. This assumption appears reasonable from the present results that the wall-proximity effect is usually dominant only at the locations where the distance from the wall to the probe center is smaller than two probe diameters. Most frequently, the five-hole probe head near the wall is placed parallel to the wall as in Fig. 1(b). Sometimes, the five-hole probe may be oriented inevitably as in Fig. 1(a) near a divergent wall and as in Fig. 1(c) over a convergent surface. The orientation angle between the wall and the probe head can also be termed as the pitch angle as in Fig. 1.

Conventional three-hole wedge probes failed to measure the correct static pressure when operating in close proximity to a wall through which the probe was inserted, yet well outside the boundary layer (Smout and Ivey, 1994, 1996a and 1996b). Contrary to the probes with a cobra-shaped stem, the wedge probe usually consists of a wedge head, an interface piece and a straight probe stem. Cook (1988) reported that the freestream static pressure near the outer wall of tur-

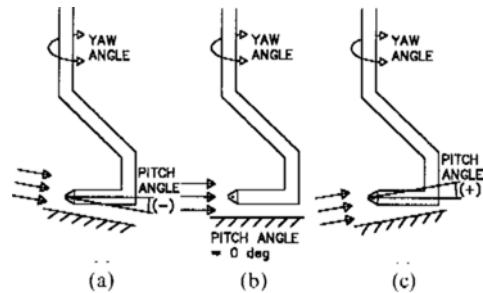


Fig. 1 Some five-hole probe orientations near the wall.

bomachines was over indicated by upto 20% dynamic head. This static-pressure wall-proximity effect was found even when the pressure sensing holes were 10 probe diameter away from the wall. Smout and Ivey (1996a) found that increasing the length of the interface piece gave a significant reduction in near-wall static-pressure measurement errors, and increased in wedge-head included angle, Mach number and pitch angle resulted in accentuated static-pressure wall-proximity effects. Through flow visualization experiments, they identified two distinct regions of recirculating flow in the wedge-probe wake, and showed that any alteration to the recirculations, by operating the probe near to the wall, would alter the static-pressure and yaw-angle measurements of the wedge probe.

There are a lot of investigations of the factors influencing the calibration of five-hole probes at the locations far away from the wall. Recently, Dominy and Hudson (1993) extensively investigated effects of the Reynolds number, Mach number and turbulent intensity on the calibration of various five-hole probes. The wall-proximity effect of a five-hole probe was firstly investigated by Treaster and Yocum (1979) for a miniature prism-type five-hole probe. It had five pressure-sensing holes on a cylindrical surface two diameter apart from the stem end and hence was actually used in the form of a cantilever, similarly to the wedge-head probes. For the five-hole probe approaching and being withdrawn normal to a knife-edged flat plate in a jet, they found that among the four calibration coefficients, only the static-pressure coefficient exhibited significant changes even in the case that a distance from the

wall to the central hole was greater than two probe diameters. The results for the prism probe, which is similar to those for the wedge probe, can not be directly applied to the near-wall measurements with a popular cone-type five-hole probe with a cobra-shaped stem, due to the totally different probe-stem arrangement.

In this study, the effect of the wall proximity on the calibration of a commonly used cone-type five-hole probe with a typical cobra-shaped probe stem is investigated for different probe-wall orientations and yaw angles. To this end, a large-scale cone-type five-hole probe was employed in a well-established laminar boundary layer. Contrary to a miniature probe, the large-scale probe offered a precise fabrication of the probe head, a negligibly small boundary-layer thickness with respect to the probe-head diameter, and an appropriate probe Reynolds number of turbomachinery flows in a low-speed wind tunnel.

## 2. Experiment

### 2.1 Large-scale cone-type five-hole probe

The five-hole probe used in this study is presented in Fig. 2. The cone angle, which was defined as an included angle at the probe tip, was fixed at a typical value of 60 deg. The probe-head diameter,  $D$ , and diameter of each pressure-sensing hole were 32mm and 4 mm, respectively. The axes of the pressure holes from #2 to #5 were perpendicular to the cone surface. The probe head of its length 80mm was made of aluminum and inserted into a cobra-shaped probe stem (Fig. 3), which was made of stainless steel pipe of 1 mm in thickness and 32 mm in outer diameter. The total length between the leading and the trailing edges of the probe was about  $4D$ . The centerline of the

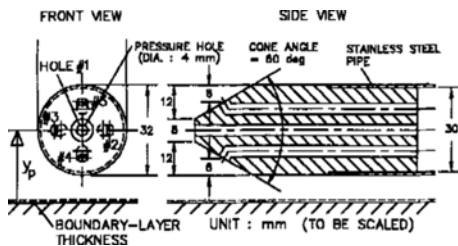


Fig. 2 Detail of present large-scale five-hole probe.

five-hole probe stem passed through the center of the hole #1 inlet, so that the probe was always positioned at the same location regardless of yaw-angle change as shown in Fig. 3.

### 2.2 Experimental apparatus and procedure

The present experimental rig was made up of a wind tunnel, a three-axis automatic probe traverse system equipped with a two-axes probe rotator, a flat plate for laminar boundary-layer development, a boundary-layer suction system and the large-scale five-hole probe. The wind tunnel was an open-circuit type with a cross-section of  $0.6m \times 0.4m$ , and its area contraction ratio was 9.0. Over the floor of the wind-tunnel test section, the flat plate with the boundary-layer suction system was located as in Fig. 3, on which a laminar boundary layer was developed. The probe was precisely positioned at each measurement location with the three-axis automatic traverse system which was equipped with linear-motion guides, stepping motors and stepping motor drivers. The two-axis probe rotator, which was installed on the traverse system, was used for the changes of the yaw and pitch angles as in Fig. 3. A pitot-static probe of 2.1 mm in a diameter, which was located sufficiently away from the five-hole probe in the spanwise direction, was also moved with the automatic traverse system, so that the two probes had the same elevation at

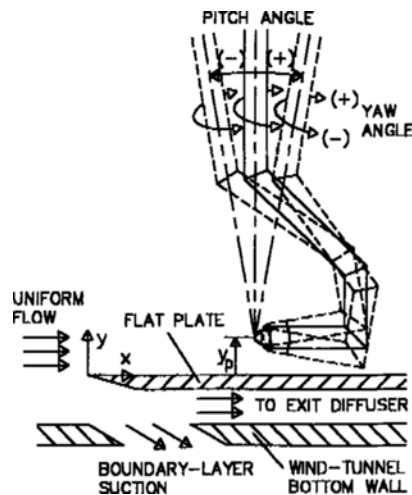


Fig. 3 Tested five hole probe near the wall.

each measurement location. In each case that the two angles were altered, the probe location was carefully adjusted.

The pressure measurement system employed in this study was basically the same as that of Lee et al. (1994 and 1997). All experiments were controlled by a personal computer (IBM, AT 486) equipped with a Multi-Function DI/O Board (National Instruments, AT-MIO-16D-H-9). The probe traverse system and pressure scanning box (Furness Controls, FC091-6) for switching the five pressure holes in sequence, were controlled by digital-out signals from the Multi-Function DI/O Board. Measured pressures were transformed into DC voltages by a high-accuracy differential pressure transducer (MKS, Type 120AD-00010RAB), in which an electric heater was installed to keep the transducer at constant temperature. The electric signals were sampled by a 12-bit A-D converter in the Multi-Function DI/O Board, and transferred into the computer. The whole measurement system was controlled in a proper sequence by a standalone C-language program.

### 2.3 Experimental conditions and uncertainties

In this study, the freestream velocity,  $U_\infty$ , was maintained to be 15.0 m/s, and the probe Reynolds numbers based on the probe-head diameter and freestream velocity,  $Re_p$ , was  $3.53 \times 10^4$ , which is a representative Reynolds number in turbomachinery. Two-dimensionality of the incoming flow was assured by measuring the velocity profiles at five spanwise locations. In order to minimize the boundary-layer thickness, the boundary layer was kept to be laminar without a leading-edge separation bubble. It was achieved by a careful adjustment of the massflow rate of the boundary-layer suction. All the experiments were performed at  $x=80$  mm, and the Reynolds number based on  $x$  and  $U_\infty$  was given to be  $Re_x=7.70 \times 10^4$ . Figure 4 shows the final boundary-layer velocity profiles along the midspan of a flat plate. The boundary-layer thickness ( $\delta_{99}$ ), displacement thickness and momentum thickness were measured to be 0.90 mm, 0.296 mm and 0.

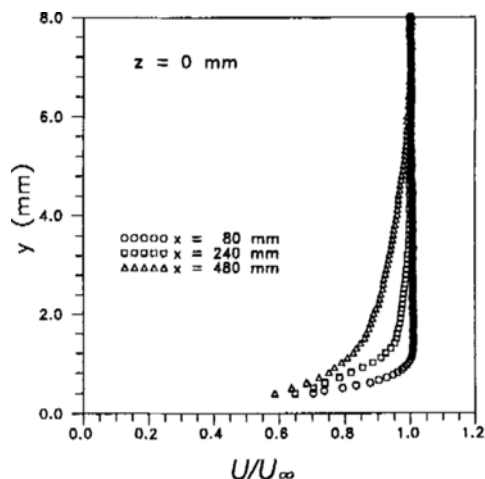


Fig. 4 Boundary-layer velocity profiles.

129 mm, respectively, at the measurement location. Therefore,  $\delta_{99}/D$  was given to be 0.028 and the relative size of the boundary-layer thickness with respect to the probe-head diameter is drawn in Fig. 2. In this experiment, the yaw angle is changed from  $-40$  deg to  $+40$  deg with an interval of 10 deg. In the case that the pitch angle is positive (Fig. 1(c), Fig. 3), there is a limitation to approach the probe close to the wall due to the presence of the probe trailing edge. On the contrary, the probe can approach very close to the wall in the case that the pitch angle is negative (Fig. 1(a), Fig. 3). For these reasons, the pitch angle was altered to be 10 deg, 0 deg,  $-10$  deg and  $-20$  deg. The wall-proximity,  $y_p$ , was defined as a distance from the wall to the center of the pressure hole #1, as in Fig. 2. For each five-hole probe orientation, the five-hole probe was traversed with an interval of 2.0 mm ( $0.0625D$ ) up to  $y_p/D=4.0$  (128mm) in the  $y$ -direction. Preliminary test for a commercially-available miniature five-hole probe (United Electric Controls, DC-125-24-F-22-CD) of about 3.2 mm in probe-head diameter showed that measurements for  $y_p > 4.0$  was not necessary.

The uncertainty intervals presented in this study were evaluated with 95 percent confidence (Abernethy et al., 1985). Uncertainties associated with the probe rotation were given to be  $\pm 0.2$  deg in the pitch angle and  $\pm 0.2$  deg in the yaw angle. The uncertainty in the pressure measurement was

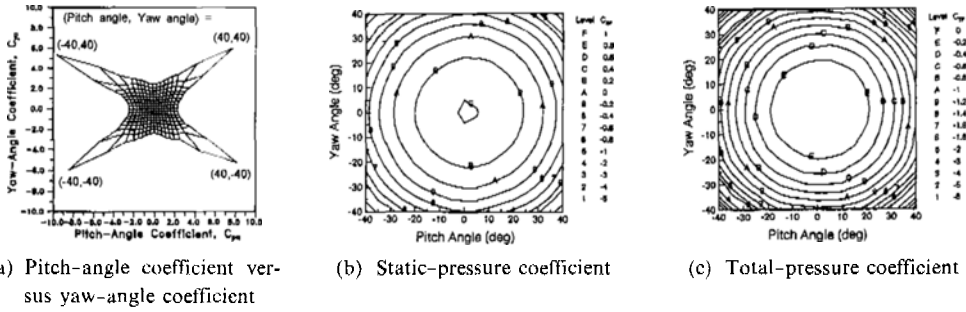


Fig. 5 Typical calibration curves without wall-proximity effect.

estimated to be  $\pm 0.7\%$  of the freestream dynamic pressure. The uncertainty intervals associated with the pitch-angle coefficient, yaw-angle coefficient, static-pressure coefficient and total-pressure coefficient were given to be  $\pm 0.120$ ,  $\pm 0.095$ ,  $\pm 0.023$  and  $\pm 0.043$ , respectively.

### 3. Result and Discussion

#### 3.1 Typical calibration coefficients in a non-nulling mode

In general, calibration coefficients of the five-hole probe in a non-nulling procedure are defined as follows (Treaster and Yocum, 1979):

Pitch-angle coefficient,

$$C_{pa} = (P_4 - P_5) / (P_1 - P_{av}) \quad (1)$$

Yaw-angle coefficient,

$$C_{ya} = (P_2 - P_3) / (P_1 - P_{av}) \quad (2)$$

Static-pressure coefficient,

$$C_{sp} = (P_{av} - P_s) / (P_1 - P_{av}) \quad (3)$$

Total-pressure coefficient,

$$C_{tp} = (P_1 - P_t) / (P_1 - P_{av}) \quad (4)$$

In the above equations,  $P_1$ ,  $P_2$ ,  $P_3$ ,  $P_4$  and  $P_5$  represent the measured pressures at the corresponding pressure holes as shown in Fig. 2, and the static pressure,  $P_s$ , and the total pressure,  $P_t$ , are usually measured by means of a pitot-static probe. The pressure,  $P_{av}$ , is defined as in eq. (5):

$$P_{av} = (P_2 + P_3 + P_4 + P_5) / 4 \quad (5)$$

Figure 5 provides the calibration coefficients for the present large-scale five-hole probe without the wall-proximity effect. They were collected at an open-circuit wind-tunnel exit in the absence of a solid wall for both pitch and yaw angles

between  $-40$  deg and  $40$  deg with an interval of  $5$  deg. When the compressibility is not considered, it is usual to determine the actual flow angles from contours of the pitch-angle coefficient and yaw-angle coefficient over the calibrated range as in Fig. 5(a). Therefore, it is essential that each pair of pitch-angle coefficient and yaw-angle coefficient should be mapped one-to-one onto the corresponding pitch and yaw angles. Once the flow direction has been established through a proper interpolation procedure, the remaining pressures can be determined from contours of the static-pressure coefficient (Fig. 5(b)) and contours of the total-pressure coefficient (Fig. 5(c)). Thus, the flow-angle determination is very important in the reduction procedure, because the reduced flow angles directly influence the subsequent pressure determinations.

#### 3.2 Effect of the wall proximity on the calibration coefficients

In Fig. 6, the calibration coefficients for the present large-scale five-hole probe are presented with the variation of the yaw angle when the pitch angle is zero. The results are very important in that this parallel probe-plate orientation as in Fig. 1(b) is most frequently encountered in actual flow measurements. For this probe-wall orientation, the wall proximity,  $y_p$ , is  $0.5D$  when the bottom surface of the five-hole probe head is in contact with the wall, and the closest measurement location is  $2\text{mm}$  apart from the wall, which is equivalent to  $y_p/D = 0.5625$ . For the whole tested yaw angles, the pitch-angle coefficient increases as the probe approaches the wall. It is noted that the general trend of  $C_{pa}$  seems to be

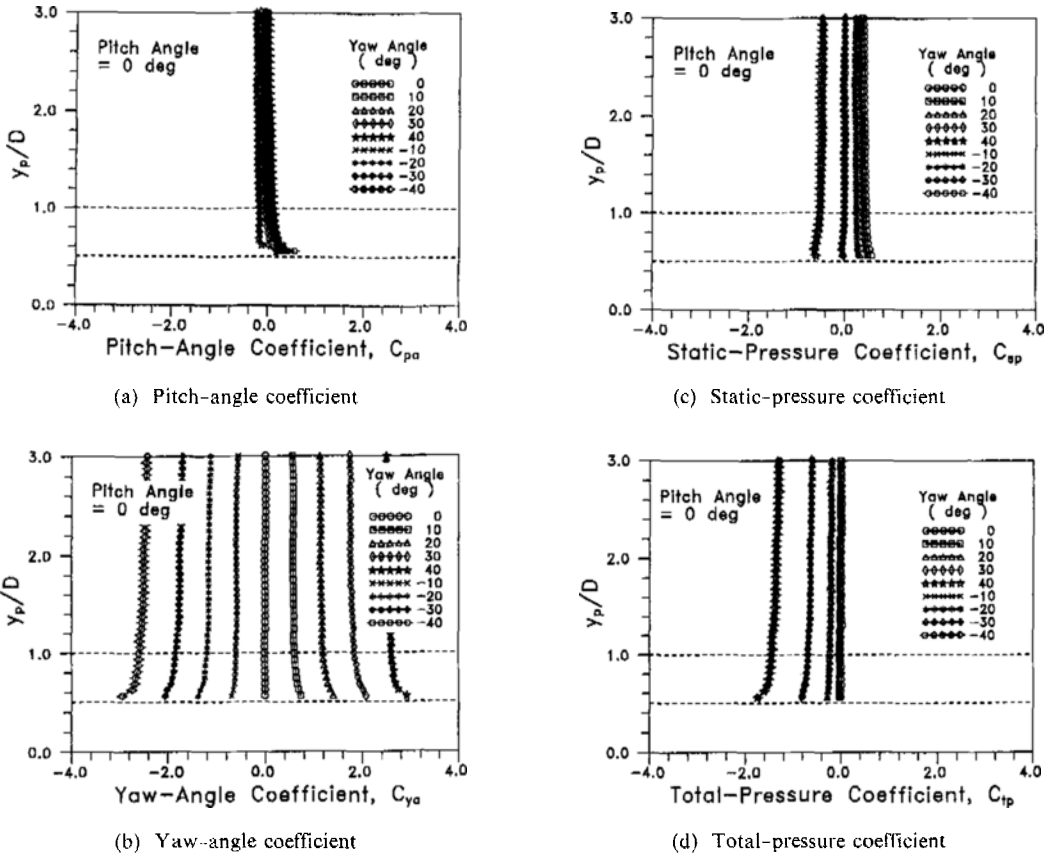
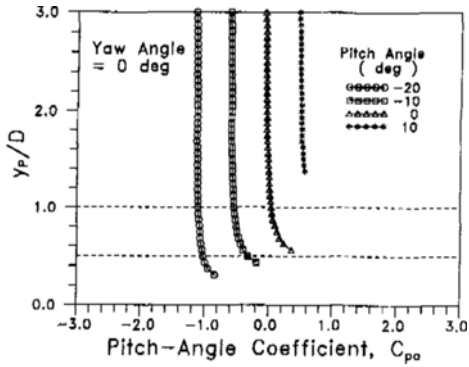


Fig. 6 Effect of wall proximity on calibration coefficients for pitch angle of 0 deg.

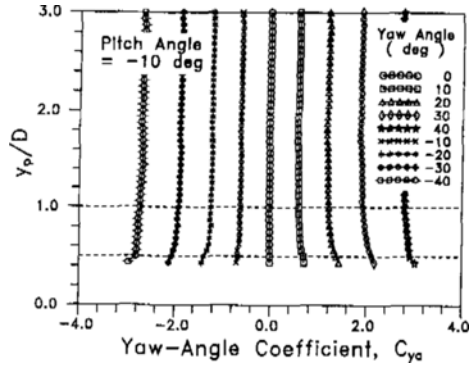
nearly independent of the yaw angle, and the increase in the pitch-angle coefficient is found to be noticeable only in the case that  $y_p/D$  is smaller than about 1.0. Due to the large wall-proximity effect even for the yaw angle of 0 deg, care should be taken in the near-wall measurement of the pitch angle, when the five-hole probe is used in a nulling mode. As the probe moves toward the wall, the yaw-angle coefficients (Fig. 6(b)) are increased for the positive yaw angles, but are decreased for the negative yaw angles. If the absolute values of the yaw angle are identical, the absolute changes in  $C_{ya}$  are nearly the same. In general, the larger yaw angle results in more sensitive variation of the near-wall  $C_{ya}$ . Particularly for the yaw angle of 0 deg, the wall-proximity effect of  $C_{ya}$  is found to be negligible in contrast with that of  $C_{pa}$ . Fig. 6(c) shows that the static-pressure coefficient,  $C_{sp}$ , is also altered near the wall, but the amount is small compared

with those of  $C_{pa}$  and  $C_{ya}$ .  $C_{sp}$  is slightly increased as the probe approaches the wall for the absolute yaw angles smaller than 20 deg, while it is decreased for the absolute values of yaw angle larger than 30 deg except for at  $y_p=0.5625$ . The total pressure coefficient (Fig. 6(d)) seems to be nearly independent of the wall proximity in the case that the absolute value of the yaw angle is less than 10 deg. As the probe moves toward the wall, the total pressure coefficient tends to decrease for the absolute yaw angles larger than 20 deg. Among the tested yaw angles, the change in  $C_{tp}$  is found to be largest when the yaw angle is 40 deg.

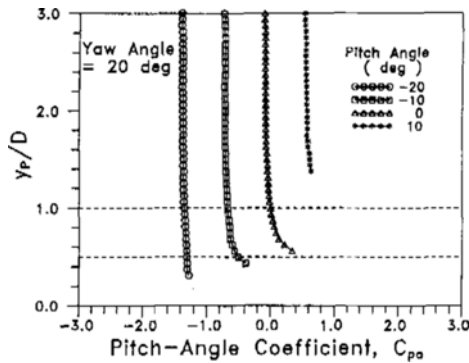
Figure 7 shows the effect of the wall proximity on the pitch-angle coefficients for various probe-wall orientations. When the pitch angle has a negative value, the probe can be moved closer toward the wall than in the case of the pitch angle of 0 deg, while for a positive pitch angle, it is



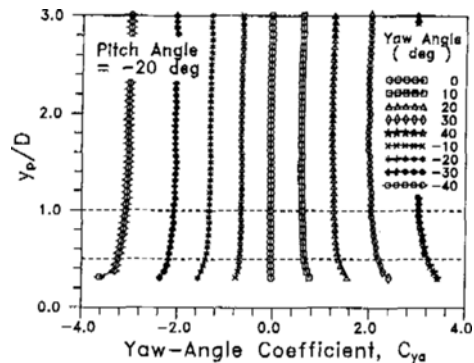
(a) Yaw angle=0 deg



(a) Pitch angle=-10 deg



(b) Yaw angle=20 deg



(b) Pitch angle=-20 deg

**Fig. 7** Effect of wall proximity on pitch-angle coefficients as a function of pitch angle.

**Fig. 8** Effect of wall proximity on yaw-angle coefficients for different pitch angles.

impossible for the wall proximity,  $y_p$ , to be smaller than about  $1D$  due to the geometrical limitation of the probe head (Fig. 1(c), Fig. 3). As the pitch angle increases from  $-20$  deg to  $10$  deg, the location, at which the wall-proximity effect of the pitch-angle coefficient is dominant, shifts away from the wall. It is noted that the wall-proximity effect is found to be minimal when the pitch angle is  $-20$  the deg. This tendency is also observed in the case of the yaw angle of  $20$  deg. Particularly for the pitch angle of  $-20$  deg, the pitch-angle coefficient is nearly independent of the wall proximity as in Fig. 7(b). Results of the yaw-angle coefficient for the pitch angles of  $-10$  deg and  $-20$  deg are presented in Fig. 8. Even for these pitch angles, effects of the wall proximity on the yaw-angle coefficient have qualitatively the same trend as that for the pitch angle of  $0$  deg (Fig. 7(b)). However, the wall-proximity effect is most

noticeable for the pitch angle of  $0$  deg at the locations between  $y_p/D=0.5$  and  $1.0$  (Fig. 6(b), Fig. 8). Effects of the wall proximity on the static-pressure coefficient for different pitch angles are nearly similar when  $y_p/D$  is larger than  $0.5$  (Fig. 6(c) and Fig. 9). Finally, for the absolute values of the yaw angle less than  $30$  deg, the wall proximity effect of the total-pressure coefficient, in general, is very weakly dependent upon the pitch angle when  $y_p/D$  is larger than  $0.5$  (Fig. 10). Even for the yaw angles of  $-40$  deg and  $40$  deg, the changes in the total-pressure coefficient are restricted to the locations where  $y_p/D$  is smaller than  $1.0$ . From the results presented in Fig. 8 to Fig. 10, it is concluded that changes in the pitch angle from  $0$  deg to  $-20$  deg result in the reduction of the wall-proximity effect on all the calibration coefficients. The profile of each calibration coefficient seems to be nearly the same, meanwhile the

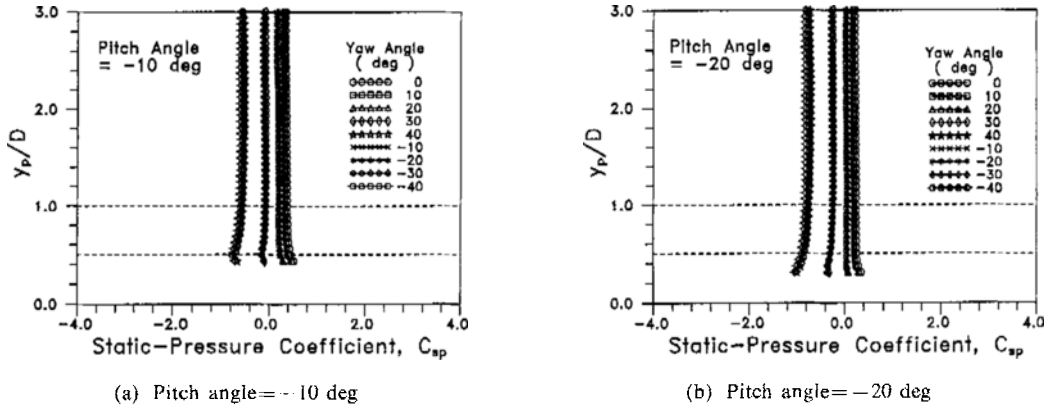


Fig. 9 Effect of wall proximity on static-pressure coefficients for different pitch angles.

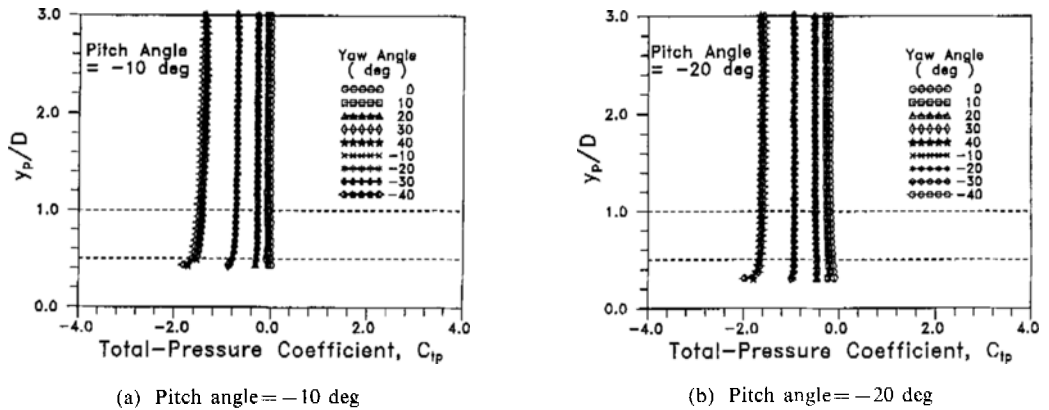


Fig. 10 Effect of wall proximity on total-pressure coefficients for different pitch angles.

location where the wall-proximity effect is dominant tends to shift toward the wall.

As mentioned in the introduction, present wall-proximity study is based on the assumption that the near-wall flow in a actual flow field is usually parallel to the wall. Fortunately, it is found from the present near-wall data that the wall-proximity effect is dominant only at the locations very close to the wall, independent of the probe-wall orientation.

**3.3 Effect of wall proximity on the pressures measured at five pressure holes**

Pressures measured at the five pressure holes when the pitch angle is 0 deg are presented for the yaw angles of 0 deg and 20 deg in a dimensionless form in Fig. 11. From the pressure data, the wall-proximity effect on the calibration coefficients can be clearly understood. For the yaw angle of 0 deg

(Fig. 11(a)), it is observed that the pressures  $P_1$ ,  $P_2$ ,  $P_3$ , and  $P_5$  are not affected by the wall proximity, while  $P_4$  is considerably increased near the wall. The increase in  $P_4$  toward the wall leads the increase in  $C_{pa}$  as in Fig. 6(a) and Fig. 7(a). In the case that the probe is far away from the wall, the flow over the cone surface tends to be axisymmetric. Hence, the pressures measured at the holes on the cone surface are identical, even though there still exists slight pressure difference between  $P_4$  and  $P_5$  under the influence of the probe stem. When the five-hole probe is located close to the wall as in Fig. 2, however, the flow near the bottom cone surface facing the wall is bounded by the wall, and the flow over the cone surface becomes three-dimensional. In the presence of the wall, the bottom portion of the cone surface effectively stagnates the on-coming flow particularly in the flow-symmetry plane. As the probe

approaches the wall, the stagnation point may migrate from the hole #1 toward the hole #4. After all, the pressure measured at the hole #4, which faces the wall, is increased as in Fig. 11(a). For a circular cylinder near a boundary layer, Bearman and Zdravkovich(1978) also showed that the stagnation point migrated toward the wall as the cylinder approached the wall. For the yaw angle of 20 deg(Fig. 11(b)), the pressures measured near the wall have somewhat different trends. Figure 11(b) shows that the pressures  $P_1$ ,  $P_3$  and  $P_5$  are slightly decreased, while  $P_2$  and  $P_4$  are increased. For this positive yaw-angle case, the hole #3 is located on the leeward side and the hole #2 exists on the windward side. The large change in  $P_4$  is also attributed to the stagnation effect as discussed in Fig. 11(a). The slight near-wall pressure increase at the hole #2 seems to be influenced by the flow stagnation as well. The

flow near the leeward side, which is intrinsically unstable, is liable to change, and may be sensitive to the change in wall-cone arrangement. Therefore, the presence of the wall easily alters the surface flow on the leeward side and tends to stimulate the flow separation from the cone, which results in decreases in even  $P_1$  and  $P_5$  as well as  $P_3$ . It is summarized from the discussions for the pitch angle of 0 deg that the wall-proximity effect is mainly occurred in two reasons. Firstly, the wall proximity effect, which usually changes the pitch-angle coefficient, is resulted mainly from the effective stagnation of the on-coming near-wall flow by the cone surface facing the wall, which leads the increase in the surface pressure. Secondly, the wall-proximity effect for large yaw angles, which is associated with the yaw-angle coefficient, is attributed to the sensitive flow change on the leeward cone surface

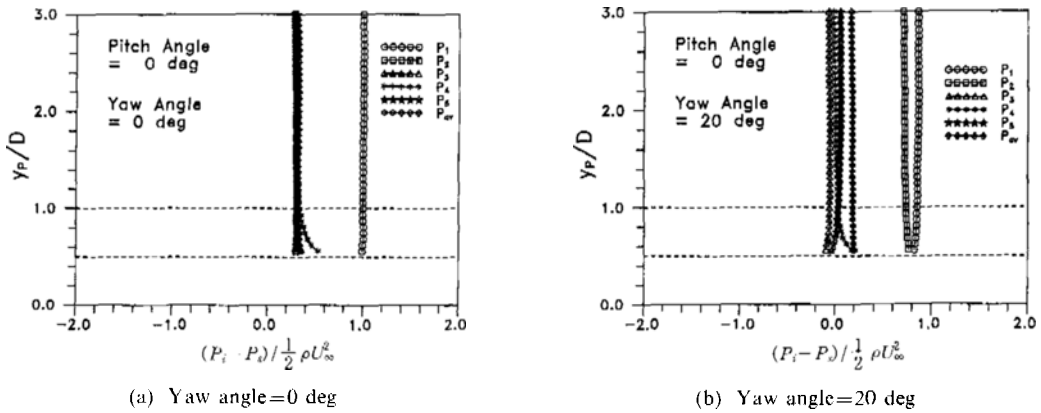


Fig. 11 Effect of wall proximity on pressures measured at five pressure holes for pitch angle of 0 deg.

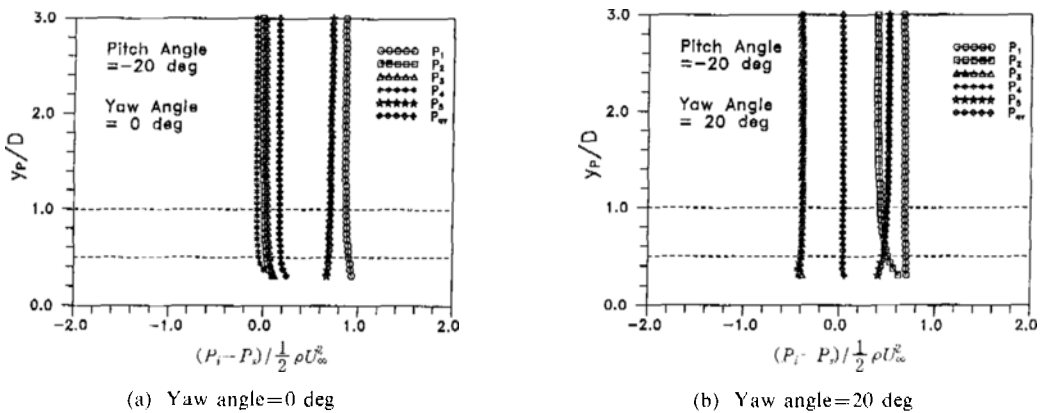


Fig. 12 Effect of wall proximity on pressures measured at five pressure holes for pitch angle of -20 deg.

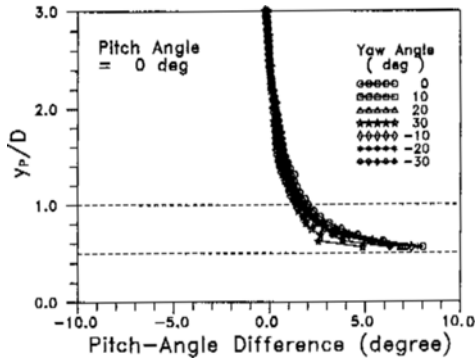
with the variation of the wall proximity.

Five pressures for the pitch angle of  $-20$  deg are presented in Fig. 12 in a dimensionless form. For the yaw angle of  $0$  deg (Fig. 12(a)),  $P_1$ ,  $P_2$ ,  $P_3$  and  $P_4$ , have increasing trends toward the wall, meanwhile  $P_5$  has an opposite tendency. Strictly speaking, the significant pressure changes in  $P_2$ ,  $P_3$  and  $P_4$  happen only at the locations where  $y_p/D$  is smaller than  $0.5$ , contrary to the change in  $P_4$  for pitch angle of  $0$  deg (Fig. 11(a)). For this slanting probe orientation, the hole #1 as well as the hole #4 face obliquely toward the wall. Therefore, the near-wall pressure increases are mainly due to the stagnation of the approaching flow as discussed in Fig. 11(a). It is inferred that the increases in  $P_2$  and  $P_3$  are resulted from an indirect influence of the flow stagnation as well. On the other hand, the decrease in  $P_5$  near the wall seems to be originated from an acceleration of the on-coming flow over the obliquely-oriented top cone surface. For the yaw angle of  $20$  deg (Fig. 12(b)), the changes in both  $P_2$  and  $P_5$  are noticeable, but  $P_{av}$  as well as  $P_1$ ,  $P_3$  and  $P_4$  suffer very little change. For this probe orientation, the hole #2 and #5 are located on the windward side, while both hole #3 and hole #4 are on the leeward side. The considerable increase in  $P_2$  may be attributed to the fact that the hole #2 is situated near the stagnation point. The decrease in  $P_5$ , which exhibits very similar trend to that of  $P_5$  for the yaw angle of  $0$  deg, is resulted from the acceleration of the on-coming flow over the top cone surface. From the above discussions for different probe-wall orientations, it is understood that the wall-proximity effects are principally originated from very complicated flow changes over the five-hole probe surface. Moreover, the effect of the yaw angle on the near-wall flow change is found to be strongly coupled with that of the probe-wall orientation.

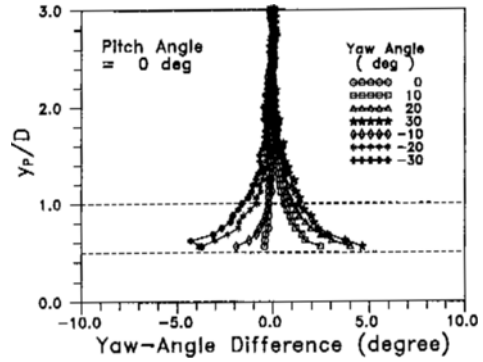
### 3.4 Effect of wall proximity on the pitch and yaw angles

In the earlier discussions, the effects of the wall proximity on the calibration coefficients were mainly presented. In addition to these, it would be very important to know the actual amount of

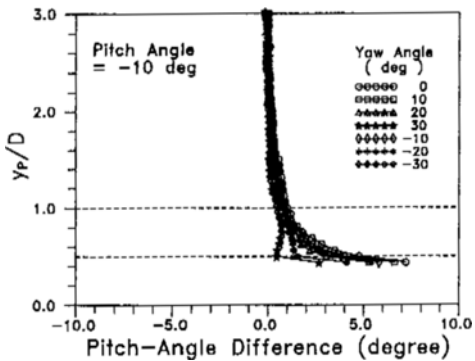
changes in the flow angles, static pressure and total pressure due to the wall proximity. In order to do this, a data reduction program, which employs a typical non-nulling method based on Treaster and Yocum (1979), has been developed. In the reduction procedure, the pitch and yaw angles are firstly obtained from the relation in Fig. 5(a), regardless of the static- and total-pressure coefficients. On the other hand, the subsequent determination of the static and total pressures are strongly dependent upon the reduced pitch and yaw angles as well as the static- and total-pressure coefficients as in Fig. 5(b) and Fig. 5(c). Five pressure data obtained in this wall-proximity experiment are converted into the corresponding pitch angle, yaw angle, static pressure and total pressure, applying the freestream calibration data in Fig. 5 to the reduction program. At the location far away from the wall, the rotated pitch and yaw angles, the freestream static pressure and freestream total pressure are obtained within uncertainty intervals. On the contrary, the pitch and yaw angles as well as the static and total pressures from the reduction program at the locations close to the wall become different from the rotated flow angles and the freestream pressures, respectively. For example, in the case of the pitch angle of  $0$  deg and the yaw angle of  $0$  deg, the reduced angle and yaw angles at  $y_p/D=0.5625$  are  $8.0$  deg and  $-0.4$  deg, respectively. The angle changes result in increase in the static pressure by  $11.3$  percent of the freestream dynamic pressure and decrease in the total pressure by  $1.8$  percent of the freestream dynamic pressure, and finally, the velocity magnitude is decreased by  $6.7$  percent of the freestream velocity. Noting the reduction procedure, the differences in the yaw and pitch angles between the reduced and rotated values are considered as the measurement errors due to the wall proximity. However, the reduced near-wall static and total pressures are resulted only from the flow-angle errors, assuming that the total- and static-pressure coefficients near the wall are always the same as the freestream ones independent of the wall proximity. Judging from the results in Fig. 6(c), Fig. 6(d), Fig. 9 and Fig. 10, the assumption is



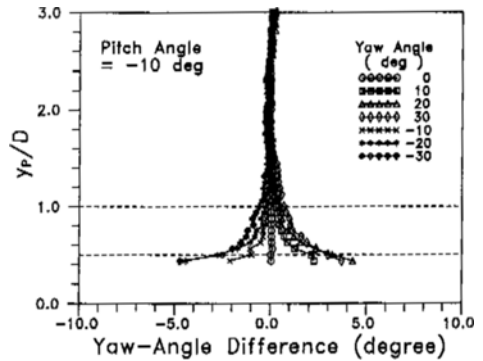
(a) Pitch angle=0 deg



(a) Pitch angle=0 deg



(b) Pitch angle=-10 deg



(b) Pitch angle=-10 deg

Fig. 13 Pitch-angle changes due to wall proximity.

Fig. 14 Yaw-angle changes due to wall proximity.

hardly acceptable near the wall. In this sense, only the changes in the pitch and yaw angles due to the wall proximity are discussed in detail.

The pitch-angle difference,  $(\alpha - \alpha_\infty)$ , is presented in Fig. 13 for the pitch angles of 0 deg and -10 deg. As can be seen in Fig. 13(a), the pitch-angle difference for the pitch angle of 0 deg tends to be increased as the probe approaches the wall, independent of the yaw angle. These trends seem to be nearly the same as those of the pitch-angle coefficient in Fig. 6(a). Exactly speaking, the pitch-angle difference for the pitch angle of 0 deg is found to be largest when the yaw angle is zero. The effect of the yaw angle on  $(\alpha - \alpha_\infty)$  seems to be minor in the case that the absolute yaw angle is smaller than 20 deg. The maximum value of  $(\alpha - \alpha_\infty)$  is 8.0 deg at  $y_p/D = 0.5625$  for the yaw angle of 0 deg. As the probe departs from the wall, the pitch-angle difference is substantially decreased. Therefore, the difference is less than

about 2 deg at  $y_p/D = 1.0$  and finally is within 0.5 deg at  $y_p/D = 2.0$ . As the pitch angle is changed from 0 deg to -10 deg, the locations with larger wall-proximity effect move closer toward the wall. Thus, the wall proximity effect for the pitch angle of -10 deg is confined to the restricted locations near the wall as in Fig. 13(b). In Fig. 14, the yaw-angle difference,  $(\beta - \beta_\infty)$ , is presented. As in Fig. 6(b), the yaw-angle difference near the wall for the pitch angle of 0 deg (Fig. 14(a)) is increased for the positive yaw angles, but is decreased for the negative yaw angles. If the absolute values of the yaw angle are identical, changes in the absolute  $(\beta - \beta_\infty)$  are approximately the same. Generally, larger yaw angle results in more sensitive variation of the near-wall  $(\beta - \beta_\infty)$ , and the maximum of the absolute values of  $(\beta - \beta_\infty)$ , which is occurred at  $y_p/D = 0.5625$  for the yaw angle of 30 deg, are about 5 deg. Particularly for the yaw angle of 0 deg, the yaw angle

difference at this probe-wall orientation is found to be very small. These tendencies of the yaw angle difference for this most frequently-encountered situation is also true for other probe-wall orientation (Fig. 14(b)). The only difference is that the location with the larger absolute value of  $(\beta - \beta_\infty)$  move closer toward the wall.

In order to account for the wall-proximity effect perfectly, the calibration data obtained at the same location from the wall as a measurement point should be applied to the reduction program with no assumption. However, it is actually impossible to realize the situation. Therefore, the most simple way to be free from the wall-proximity effect may be to avoid the near-wall measurement in reference to the results in Fig. 13 and Fig. 14. In case that the flow field near the wall should be known, it is recommended that the flow field should be made in a large scale compared to the probe size, or a miniaturized five-hole probe should be employed for a given scale flow field. Finally, it is suggested that the five-hole probe should be away from the wall by two times of the probe-head diameter, in order that the variations of the pitch and yaw angles with the wall proximity are within 0.5 deg for the parallel probe-wall orientation. This suggestion can also be applicable to other probe-wall orientations as in Fig. 1(a).

#### 4. Conclusion

Effects of the wall proximity on the calibration of a typical cone-type five-hole probes with a cobra-shaped probe have been investigated for various probe-wall orientations with the variation of the yaw angle. In order to obtain a negligibly small boundary-layer thickness to the probe-head diameter, a large-scale five-hole probe was employed in a well-established laminar boundary layer, and the probe Reynolds number was kept to be  $3.53 \times 10^4$ , which is a representative Reynolds number in turbomachinery flows. The results in this study are summarized as follows.

(1) For the probe head parallel to the wall, the wall proximity effect is mainly occurred from two different origins: Firstly, the wall proximity

effect is resulted from the effective stagnation of the on-coming near-wall flow by the cone surface facing the wall, and secondly, it is attributed to the sensitive flow change on the leeward cone surface especially for large yaw angles, depending on the wall proximity.

(2) The wall-proximity effect is remarkably influenced by the probe-wall orientation. In general, larger orientation angle between the wall and the probe head results in less wall-proximity effect.

(3) Effects of the wall proximity on the calibration coefficients of the five-hole probe are found to be pronounced only when the wall proximity is smaller than two times the probe-head diameter for the tested probe-wall orientations.

(4) In this study, measurement errors in the pitch and yaw angles due to the wall proximity are evaluated through a typical non-nulling reduction procedure. The results provide a useful guideline in the near-wall measurement using the five-hole probe.

#### Reference

- Abernethy, R. B., Benedict, R. P. and Dowdell, R. B., 1985, "ASME Measurement Uncertainty," *ASME Journal of Fluids Engineering*, Vol. 107, pp. 161~164.
- Bearman, P. W. and Zdravkovich, M. M., 1978, "Flow around a Circular Cylinder near a Plane Boundary," *Journal of Fluid Mechanics*, Vol. 89, pp. 33~47.
- Cook, S. C. P., 1988, *Measurement Techniques for Unsteady Turbomachinery Flows*, Ph. D. Thesis, Cranfield University, Bedford.
- Dominy, R. G. and Hodson, H. P., 1993, "An Investigation of Factors Influencing the Calibration of Five-Hole Probes for Three-Dimensional Flow Measurement," *ASME Journal of Turbomachinery*, Vol. 115, pp. 513~519.
- Lee, S. W., Lee, J. S. and Ro, S. T., 1994, "Experimental Study on the Flow Characteristics of Streamwise Inclined Jets in Crossflow on Flat Plate," *ASME Journal of Turbomachinery*, Vol. 116, pp. 97~105.

Lee, S. W., Kim, Y. B. and Lee, J. S., 1997, "Flow Characteristics and Aerodynamic Losses of Film-Cooling Jets with Compound Angle Orientations," *ASME Journal of Turbomachinery*, Vol. 119, pp. 310~319.

Smout, P. D. and Ivey, P. C., 1994, "Wall Proximity Effects in Pneumatic Measurement of Turbomachinery Flows," *ASME paper 94-GT-116*.

Smout, P. D. and Ivey, P. C., 1996a, "Investigation of Wedge-Probe Wall-Proximity Effects-

Part 1: Experimental Study," to appear in the *ASME Journal of Turbomachinery*, ASME paper 96-GT-146.

Smout, P. D. and Ivey, P. C., 1996b, "Investigation of Wedge-Probe Wall-Proximity Effects-Part 2: Numerical and Analytical Modeling," to appear in the *ASME Journal of Turbomachinery*, ASME paper 96-GT-147.

Treaster, A. L. and Yocum, A. M., 1979, "The Calibration and Application of Five-Hole Probes," *ISA Transactions*, Vol. 18, pp. 23~34.